# Upper-bounds on qubit coherence set by master clock instabilities

Harrison Ball[1], William D. Oliver[2,3], and Michael J. Biercuk[1]
[1] *ARC Centre for Engineered Quantum Systems, School of Physics, The University of Sydney, NSW 2006 Australia*
[2] *Department of Physics, Massachusetts Institute of Technology, Cambridge, MA 02139 USA*
[3] *MIT Lincoln Laboratory, 244 Wood Street, Lexington, MA 02420, USA*

(Dated: January 10, 2016)

Distribution A: Public Release. The Lincoln Laboratory portion of this work was sponsored by the Assistant Secretary of Defense for Research & Engineering under Air Force Contract #FA8721-05-C-0002. Opinions, interpretations, conclusions and recommendations are those of the author and are not necessarily endorsed by the United States Government.

# Upper-bounds on qubit coherence set by master clock instabilities

Harrison Ball,[1] William D. Oliver,[2,3] and Michael J. Biercuk[1]

[1]*ARC Centre for Engineered Quantum Systems, School of Physics, The University of Sydney, NSW 2006 Australia*
[2]*Department of Physics, Massachusetts Institute of Technology, Cambridge, MA 02139 USA*
[3]*MIT Lincoln Laboratory, Lexington, MA 02420 USA*

(Dated: January 10, 2016)

Experimentalists seeking to improve the coherent lifetimes of quantum bits have generally focused to date on addressing their respective leading decoherence mechanisms through, for example, improvements to qubit designs, materials, and system isolation from extrinsic perturbations. In the case of the phase degree of freedom in a quantum superposition, however, the coherence that must be preserved ultimately includes that of the qubit *relative* to the system clock. In this manuscript we clarify the impact of clock instability on qubit dephasing and provide quantitative estimates of fidelity upper-bounds set by noisy phase fluctuations *in the clock*. We first demonstrate analytically that phase fluctuations in the clock - a master oscillator typically implemented and referred to as the "local oscillator" (LO) - is indistinguishable from a pure dephasing field arising from other environmental mechanisms. Using these results, we then apply commonly quoted LO *phase-noise* specifications to rigorously calculate performance bounds on qubit operational fidelities due to LO phase fluctuations. We find that for state-of-the-art performance specifications, phase fluctuations at frequencies far from the carrier dominate operational error rates. Furthermore, the control bandwidth impacts the degree to which thermal noise forms an effective phase-error floor. Our results motivate additional research directions needed in support of quantum information systems and highlight challenges and advantages that particular qubit technologies possess in the context of phase-noise induced errors.

## I. INTRODUCTION

Dephasing in qubit systems is commonly induced by environmental fluctuations of a qubit bias or control parameter, e.g., an external magnetic field, which modulates the qubit-state energy splitting and hence its dynamic evolution. In turn, experimentalists have accordingly focused their efforts on reducing both the level of environmental noise and the qubit sensitivity to that which remains. As a result of these efforts, the performance of various qubit technologies [1] has grown over recent years, and dephasing times are now measured on timescales approaching milliseconds or even seconds [2–8] with operational fidelities now reaching $99.999\%$ [9–11]. At these performance levels, noise in the control system emerges as an important contributor to the error rate, and it will eventually become a leading dephasing mechanism as the quantum information community continues to mitigate other residual error sources.

In this manuscript we identify dephasing noise induced by master-clock phase fluctuations as a potentially significant source of error in today's qubit systems and one that will certainly become more prominent as error rates improve. We express the effective dephasing Hamiltonian in terms of *LO phase fluctuations*, establishing the correspondence between common engineering measures for LO single-sideband *phase noise* and the power spectral density of the effective dephasing noise field. We unify familiar concepts from quantum information, frequency metrology, and precision oscillator characterization in order to translate phase noise specifications into gate error probabilities for a variety of canonical single-qubit operations via the filter transfer function framework. Our work highlights the fact that effective dephasing errors arising from the phase fluctuations in commonly used commercial LOs are becoming a significant consideration in the context of quantum information across qubit modalities. Specifically, our calculations demonstrate that far-from-carrier phase noise in state-of-the-art LOs provides a challenging upper bound on operational fidelities and that the bandwidth of transmitted thermal noise determines a non-negligible contribution to this error rate. Furthermore, dephasing errors due to the high-frequency portion of the phase fluctuation spectral density is not efficiently addressed through dynamic error suppression, mandating improvements in LO hardware for long-term performance gains.

## II. RESULTS

In a semiclassical picture, qubit phase coherence corresponds to maintaining the dynamical phase of the qubit *relative* to a reference (master) clock for the system. Implicit in the Bloch sphere representation of a qubit's state is, in general, a transformation to a frame co-rotating with the nominal qubit Larmor frequency. Any frequency difference $\Delta(t)$ between these two effective oscillators (the clock and the qubit) will result in phase accumulation $\phi(\tau) = \int_0^\tau \Delta(t)dt$ in the rotating frame. In a dephasing process, $\Delta(t)$ evolves stochastically in time, introducing a degree of randomness to the phase evolution over a time period $\tau$. This simple observation indicates that not only must an experimentalist consider the stability of the qubit itself, but also the stability of the rotating frame realized through use of a local oscillator (LO) in the experiment.

We demonstrate this observation formally by considering an ensemble of identically prepared noninteracting qubits subjected to a noisy environment and an external controller. Following our previous work these dynamics may be incorporated by specifying the generalized time-dependent Hamilto-

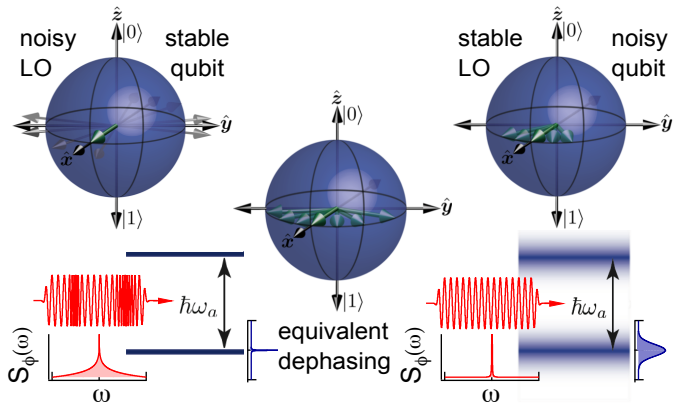


FIG. 1. Schematic representation of the correspondence between phase fluctuations and extrinsic dephasing. A stable qubit interacting with a LO experiencing frequency instability (captured by the *phase instability*, $S_\phi(\omega)$, that is, the power spectral density of phase fluctuations), induces random phase accumulation in a freely evolving qubit, represented in the Bloch sphere picture. The same phenomenology arises for a LO outputting a perfectly stable sinusoidal signal in the presence of extrinsic Hamiltonian terms that produce uncertainty in the frequency of the qubit transition.

nian as the sum of control and noisy components

$$H(t) = H_c(t) + H_0(t) \tag{1}$$
$$= \mathbf{h}(t)\boldsymbol{\sigma} + \boldsymbol{\eta}(t)\boldsymbol{\sigma}. \tag{2}$$

Here $\boldsymbol{\sigma}$ denotes a column vector of Pauli matrices and the row vectors $\mathbf{h}(t), \boldsymbol{\eta}(t) \in \mathbb{R}^3$ denote respectively the Cartesian components of the control Hamiltonian, $H_c(t)$, and noise Hamiltonian, $H_0(t)$, in the basis of Pauli operators [12, 13].

This formulation assumes an interaction picture co-rotating with the (resonant) driving field. In this picture the components $h_i(t)$, $i \in \{x, y, z\}$, of the control field relate directly to the instantaneous Rabi rate $\Omega(t) = 2\|\boldsymbol{h}(t)\|$, while the stochastic noise fields $\eta_i(t)$, $i \in \{x, y, z\}$ model semi-classical time-dependent perturbations in each of the three spatial directions. In particular, dephasing processes are captured through the noise field $\eta_z(t)$ describing stochastic evolution along $\hat{\sigma}_z$.

In this work we show the formal equivalence, in the appropriate interaction picture, of extrinsic dephasing noise processes, and intrinsic phase fluctuations *in the control device itself*. That is, setting $\eta_{x,y} = 0$ to restrict attention to the dephasing noise quadrature, we show the total Hamiltonian takes the form

$$H(t) = \mathbf{h}(t)\boldsymbol{\sigma} + \eta_z(t)\hat{\sigma}_z, \quad \eta_z(t) = \eta_z^{(0)}(t) + \eta_z^{(\mathrm{LO})}(t) \tag{3}$$

where the effective dephasing term consists of an extrinsic dephasing field, $\eta_z^{(0)}(t)$, and an intrinsic phase-fluctuation-induced field, $\eta_z^{(\mathrm{LO})}(t)$, on formally equal footing.

We model a qubit with nominal transition (angular) frequency $\omega_a$, driven by a local oscillator with carrier frequency $\omega_{\mathrm{LO}}$, and write the system Hamiltonian ($\hbar = 1$) in the laboratory frame

$$H_S = \frac{1}{2}\omega_a\hat{\sigma}_z + \frac{1}{2}\delta\omega_a(t)\hat{\sigma}_z + \Omega(t)\cos\Big(\omega_{\mathrm{LO}}t + [\phi_C(t) + \phi_N(t)]\Big)\hat{\sigma}_x. \tag{4}$$

The first term corresponds to the Hamiltonian of the qubit under free evolution, while the second term captures environmental noise (e.g. magnetic field fluctuations) effectively transforming the nominal energy splitting as

$$\omega_a \to \omega_a + \delta\omega_a(t). \tag{5}$$

The third term corresponds to the qubit-field interaction with amplitude $\Omega(t)$ driven by a local oscillator with nominal carrier frequency $\omega_{\mathrm{LO}}$, and with time-dependent phase formally partitioned into a "control" component (desired phase evolution), $\phi_C(t)$, and a "noise" component (unwanted phase evolution), $\phi_N(t)$. Thus, in the lab frame, extrinsic noise is captured by $\delta\omega_a(t)$ while intrinsic noise *in the LO* resides in the LO *phase fluctuation* field $\phi_N(t)$.

Moving to the interaction picture co-rotating with the carrier frequency and making the rotating-wave approximation we obtain

$$H_I^{(\omega_{\mathrm{LO}})} = \frac{1}{2}(\omega_a - \omega_{\mathrm{LO}})\hat{\sigma}_z + \frac{1}{2}\delta\omega_a(t)\hat{\sigma}_z + \frac{1}{4}\Omega(t)\Big\{e^{-i[\phi_C(t)+\phi_N(t)]}\hat{\sigma}_+ + e^{i[\phi_C(t)+\phi_N(t)]}\hat{\sigma}_-\Big\} \tag{6}$$

where we define the qubit ladder operators $\hat{\sigma}_\pm = \hat{\sigma}_x \pm i\hat{\sigma}_y$.

The LO phase fluctuation produces an effective time-dependent *frequency detuning* through its time derivative, $\delta\omega_{\mathrm{LO}}(t) = \dot{\phi}_N(t)$. That is, the LO phase fluctuation effectively transforms the LO frequency as

$$\omega_{\mathrm{LO}} \to \omega_{\mathrm{LO}} + \delta\omega_{\mathrm{LO}}(t). \tag{7}$$

In order to make this phenomenology explicitly comparable with extrinsic dephasing, we perform a second interaction-picture transformation

$$H_I^{(\omega_{\mathrm{LO}},\dot{\phi}_N)} \equiv U_{\dot{\phi}_N}^\dagger H_I^{(\omega_{\mathrm{LO}})} U_{\dot{\phi}_N} - H_{\dot{\phi}_N} \tag{8}$$

where $U_{\dot{\phi}_N}(t) = \exp[-i\frac{\phi_N(t)}{2}\hat{\sigma}_z]$ is the evolution operator under the LO-noise-induced dephasing Hamiltonian $H_{\dot{\phi}_N} \equiv \frac{1}{2}\dot{\phi}_N(t)\hat{\sigma}_z$. Setting the carrier detuning to zero, $\omega_a - \omega_{\mathrm{LO}} = 0$, the transformed system Hamiltonian subject to noisy LO phase fluctuations thereby takes the form

$$H_I^{(\omega_{\mathrm{LO}},\dot{\phi}_N)} = \frac{1}{2}\delta\omega_a(t)\hat{\sigma}_z - \frac{1}{2}\dot{\phi}_N(t)\hat{\sigma}_z + \frac{1}{2}\Omega(t)\Big\{\cos[\phi_C(t)]\hat{\sigma}_x + \sin[\phi_C(t)]\hat{\sigma}_y\Big\}. \tag{9}$$

Comparing Eq. 9 with Eq. 3 we see $\eta_z^{(0)}(t) = \frac{1}{2}\delta\omega_a(t)$ and

$\eta_z^{(\mathrm{LO})}(t) = -\frac{1}{2}\dot{\phi}_N(t) = -\frac{1}{2}\delta\omega_{\mathrm{LO}}(t)$, while the third term in Eq. 9 corresponds to the control component $\mathbf{h}(t)\boldsymbol{\sigma}$. Arriving at this expression reveals the phase fluctuation $\phi_N(t)$ in the LO produces net rotations about $\hat{\sigma}_z$ through its time derivative, $\dot{\phi}_N(t)$. This observation explicitly links LO phase fluctuations to a dephasing Hamiltonian in a manner that is *indistinguishable* from the presence of an extrinsic bath Hamiltonian $H_0(t) = \eta_z(t)\hat{\sigma}_z$. This correspondence is captured schematically in Fig. II. Importantly, once the relative phase relationship between the qubit and LO is established via some interaction (the global phase difference at $t = 0$ is irrelevant), even for times when $\Omega(t) \to 0$ this Hamiltonian can produce effective dephasing of the qubit.

The temporal nature of LO phase fluctuations motivates the use of the experimentally validated [14–16] filter transfer function formalism for calculating the impact of this effective dephasing field on qubit operational fidelities (including the identity operator - memory). For a system Hamiltonian in the form of Eq. 3 the fidelity of an arbitrary operation on $SU(2)$ is approximated in terms of the overlap integral of $S_z(\omega)$, the power spectral density (PSD) of the dephasing field $\eta_z(t)$, and $G_{z,l}(\omega)$, for $l \in \{x, y, z\}$, the filter transfer functions capturing the action of the applied control Hamiltonian $H_c(t) = \mathbf{h}(t)\boldsymbol{\sigma}$ [13, 17].

In the remainder of this paper we ignore extrinsic dephasing by setting $\eta_z^{(0)}(t) = 0$, thus restricting attention to dephasing induced by the LO. In this case $S_z(\omega)$ refers to the power spectral density of the dephasing field $\eta_z(t) = \eta_z^{(\mathrm{LO})}(t) = -\frac{1}{2}\dot{\phi}_N(t)$. However, the noise performance of a LO is typically characterized in terms of the *single-sided phase noise*, $\mathcal{L}(\omega) \equiv \frac{1}{2}S_{\phi_N}^{(1)}(\omega)$ expressed in dBc/Hz, where $S_{\phi_N}^{(1)}(\omega)$ is the *phase instability*, defined as the *unilateral* PSD of the LO phase fluctuations, $\phi_N(t)$. In this paper we include superscripts $(1)$ or $(2)$ to denote unilateral (one-sided) and bilateral (two-sided) PSDs respectively. For $\omega \geq 0$ the unilateral PSD is simply twice the value of the bilateral PSD, representing the double-sideband spectral density in the positive frequency domain (see Appendix C 2). To understand how $\mathcal{L}(\omega)$ maps to $S_z^{(1)}(\omega)$, we first define the bilateral PSD for phase fluctuations (see Appendix C 1)

$$S_{\phi_N}^{(2)}(\omega) \equiv \lim_{T\to\infty} \frac{1}{2T}\left\langle |\Phi_T(\omega)|^2 \right\rangle, \tag{10}$$

$$\Phi_T(\omega) \equiv \int_{-T}^{T} \phi_N(t) e^{-i\omega t} dt, \tag{11}$$

where $\langle\cdot\rangle$ denotes an ensemble average and the PSD is defined symmetrically over $\omega \in (-\infty, \infty)$. The second line defines the truncated Fourier transform of $\phi_N(t)$, where $[-T, T]$ is an experimental time window over which phase fluctuations are measured. $\Phi_T(\omega')$ is an estimate of the weight of the Fourier component of $\phi_N(t)$ at frequency $\omega'$, generating sidebands on the carrier at frequencies $\omega_{\mathrm{LO}} \pm \omega'$. Let the power in the LO carrier be written $\frac{1}{2}(\Omega/\gamma)^2$, where the coupling factor $\gamma \leq 1$ converts from the amplitude of the LO, $\Omega/\gamma$, to the Rabi rate, $\Omega$. Then the power in $S_{\phi_N}^{(1)}(\omega) = 2S_{\phi_N}^{(2)}(\omega)$ integrated over a 1 Hz band centred on $\omega'$ is interpreted as the ratio of the power in these sidebands relative to $\frac{1}{2}(\Omega/\gamma)^2$ (see Appendix C 4).

The phase noise $\mathcal{L}(\omega)$ is typically represented in logarithmic units of dBc/Hz as a function of frequency. We denote this by $\tilde{\mathcal{L}}(\omega) = 10\log_{10}[\mathcal{L}(\omega)]$ to indicate logarithmic units, see Fig. IIa). Following the above discussion, the Fourier frequency $\omega$ in the phase noise is *offset* from the carrier, with the units dBc/Hz indicating the sideband power value relative to the carrier measured over a 1 Hz band.

We convert from $\tilde{\mathcal{L}}(\omega)$ into linear units via the relationship $S_{\phi_N}^{(1)}(\omega) = 2 \cdot 10^{\frac{\tilde{\mathcal{L}}(\omega)}{10}}$. As demonstrated above the time-derivative of the phase is related directly to a time-dependent detuning, and we may relate their noise spectra as $\frac{1}{4}\omega^2 S_{\phi_N}^{(1)}(\omega) = S_z^{(1)}(\omega)$ (see Appendix C 1). The ultimate relationship therefore takes tabulated single-sideband phase-noise specifications to unilateral dephasing power spectral densities as

$$S_z^{(1)}(\omega) = \frac{1}{2}\omega^2 10^{\frac{\tilde{\mathcal{L}}(\omega)}{10}}. \tag{12}$$

This correspondence captures well-known [18] relationships between frequency and phase fluctuations in precision oscillator characterization and is represented graphically in Fig. IIa.

These quantities may be directly incorporated into expressions for the fidelity of arbitrary single-qubit operations in the presence of pure-dephasing noise using [13]

$$\mathcal{F}_{av}(\tau) \approx \frac{1}{2}\left\{1 + \exp[-\chi(\tau)]\right\}, \tag{13}$$

$$\chi(\tau) = \left(\frac{1}{\pi}\right)\int_0^\infty \frac{d\omega}{\omega^2} S_z^{(1)}(\omega) \sum_{l\in\, x,y,z} G_{z,l}(\omega) \tag{14}$$

$$= \left(\frac{1}{4\pi}\right)\int_0^\infty d\omega S_{\phi_N}^{(1)}(\omega) \sum_{l\in\, x,y,z} G_{z,l}(\omega) \tag{15}$$

$$= \left(\frac{1}{2\pi}\right)\int_0^\infty d\omega 10^{\frac{\tilde{\mathcal{L}}(\omega)}{10}} \sum_{l\in\, x,y,z} G_{z,l}(\omega). \tag{16}$$

The transfer functions for the control, $G_{z,l}(\omega)$, may be calculated analytically and have contributions along all Cartesian directions (indexed by $l$), as dephasing noise present during a non-commuting control operation (e.g. $H_c \propto \hat{\sigma}_x$) induces both dephasing and amplitude-damping rotations [13, 17]. The latter two expression for $\chi(\tau)$ simply re-express the overlap integral in terms of various quantities encountered in describing phase noise.

We now use these relationships to perform a quantitative exploration of the impact of LO phase noise on the fidelity of qubit operations. To calculate the operational *infidelity*, $1 - \mathcal{F}_{av}(\tau)$, we insert the published phase noise specifications for common synthesizers in the microwave X-band, together with the analytic filter transfer functions as inputs for Eq. 16. We consider two simple classes of operation: the Identity, $\hat{\mathbb{I}}$, and a driven rotation by angle $\pi$ about the $\hat{x}$-axis, $\hat{X}$. In each case we calculate the relevant terms $G_{z,l}(\omega)$ following techniques in [13, 16, 17, 19–22] (see Appendix B). These choices are representative of the broad range of operations required in e.g. the single-qubit subset of a universal

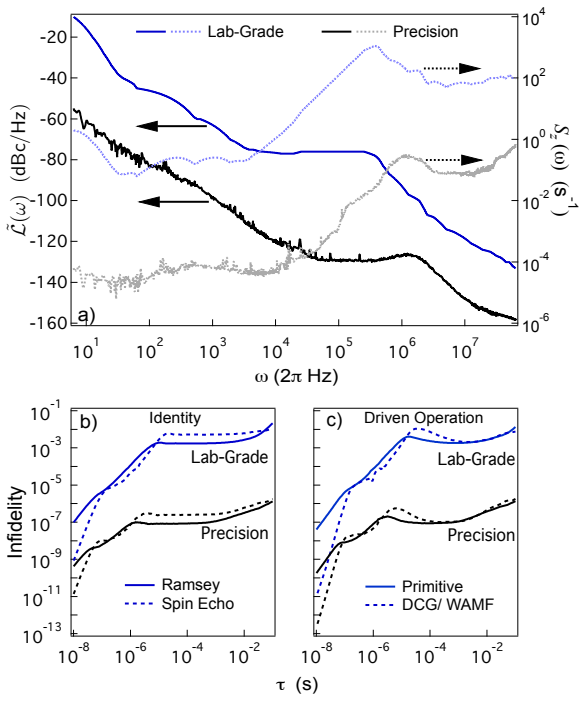


FIG. 2. a) Local oscillator phase noise expressed as $\tilde{\mathcal{L}}(\omega)$ (left axis, dark lines) and converted to $S_z^{(1)}(\omega)$ (right axis, light lines) for two grades of synthesizer. Data extracted from specification sheets and manufacturer measurements. For "lab-grade" synthesizer phase noise for offsets $\omega/2\pi < 10$ Hz data are extrapolated by the manufacturer. b-c) Calculated infidelity for different classes of quantum logic operations (see main text). We have numerically confirmed that for evolution times $\tau < 100$ ms the presence of a sharp low-frequency cutoff below $\omega/2\pi < 1$ Hz has a negligible effect on calculations relative to extrapolating existing scaling in $\tilde{\mathcal{L}}(\omega)$.

gate set. The former allows insight into the coherent lifetime (often $T_2$) of the qubit under free evolution while the latter informs how non-commuting gate fidelity is reduced by the presence of LO-induced dephasing noise.

We also compare the performance of dynamic error suppression (DES) strategies [23–38] in reducing errors due to typical phase noise, through application of time-dependent modulation of the system's dynamics with the aim of coherently averaging out slow fluctuations. While these protocols have typically been associated with the mitigation of environmental decoherence, a growing body of literature has shown that errors induced by imperfect control – including LO phase noise – can also be mitigated using the same techniques [4, 14, 16]. In our case, the analytic form for the DES version of the identity is given for spin echo, while for a driven rotation by angle $\pi$ (again $\propto \hat{\sigma}_x$), we employ a form defined as both a *dynamically corrected gate* [34–36] and a *Walsh amplitude modulated filter* [16, 39]. Full analytic expressions for these filter functions may be found in Appendix B.

For this analysis we have selected two distinct grades of LO to demonstrate the significance of LO choice in quantum control experiments. Figure IIa shows the single-sideband phase noise at 10 GHz for both a "lab grade" synthesizer (Vaunix LMS-123) and a "precision" synthesizer (Keysight/Agilent 8267D OPT-UNY). Across much of the band, as expected, the phase noise for the precision synthesizer is approximately 40 dB lower than the lab-grade unit. For the synthesizers studied here $\tilde{\mathcal{L}}(\omega)$ declines rapidly with offset frequency from the carrier, exhibiting various power-law-dependences. Details of the origins of the underlying processes may be found in [40].

Calculations of infidelity for the four operations outlined above are presented in Fig. IIb-c and summarized in Table I. For the identity operator we find an approximate improvement of $10^4$ in residual error rate due to use of a high-precision frequency source, and the infidelity remains below $10^{-6}$ out to 100 ms evolution time. By contrast the lab-grade synthesizer induces an error exceeding $\sim 0.1\%$ beyond a few microseconds of evolution time. These findings are relevant for trapped-ion [41], superconducting [42], and semiconductor [43] qubits. The plateau-like behavior in infidelity with increasing evolution time is due to the interplay of the power spectrum and filter-function [44], and is similar to phase-error saturation phenomenology observed in precision oscillator characterization [40].

In both free evolution and driven operations the deleterious impact of using a lab-grade synthesizer increases as the duration of the operation grows. For instance, for driven operations as long as 100 $\mu$s, particularly relevant for atomic qubits, the precision synthesizer only induces an error $\sim 10^{-7}$ while the lab-grade synthesizer induces an error more than $20,000\times$ larger, reaching $\sim 0.2\%$. The primary reason for this behavior is the enhanced far-from-carrier phase-noise performance in the precision synthesizer, especially over the band from approximately $1 - 1000$ kHz offset.

An interesting observation is that in the presence of these noise power spectral densities and the realistic evolution times selected for our calculations, DES protocols have a minimal effect on gate performance. Only for very short driven operations (<100 ns) does DES provide performance enhancements, where for gates with $\tau < 20$ ns error rates are suppressed more than $1000\times$. By contrast, implementing the identity operator over most of the range $\tau \in \{1\mu\text{s}, 100\text{ms}\}$ the use of spin echo actually *degrades* operational fidelity.

This is explained by considering that while $\tilde{\mathcal{L}}(\omega)$ appears to decline rapidly with offset frequency, transforming this spectrum to $S_z^{(1)}(\omega)$ (Fig. IIa, right axis) reveals the high-frequency dominance of the resulting dephasing noise, reflecting an approximately *Ohmic* spectrum ($S_z \propto \omega$) [45, 46]. In this regime DES is known to perform inefficiently as the noise evolves rapidly compared to the control and the physics of coherent averaging fails: a violation of the so-called decoupling limit.

Thermal noise in oscillators imposes a lower-error bound to be considered; even if LO hardware were improved we could do no better than saturating the thermal noise floor across the control bandwidth. This is generically quoted as -174 dBm/Hz for a matched load at 290K. This is an *absolute* noise power, meaning that for LOs with power 0 dBm the single-sideband phase noise floor will take a value $\tilde{\mathcal{L}}_{min} = -174$ dBc/Hz, and it will rise (worsen) with decreasing LO power. Higher-

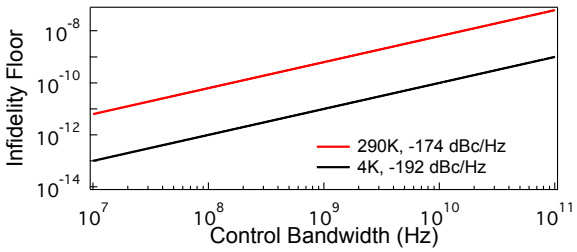


FIG. 3. Calculated infidelity floor (fidelity ceiling) imposed by thermal noise at 4K and 290K with variable control bandwidths. This calculation is independent of operation length, $\tau$ under the conditions outlined in the main text. Results hold for Ramsey and both primitive and WAMF $\pi$ rotations. Infidelity floor for spin echo is three times larger. See Appendix D

power LOs can in principle have lower phase-noise floors, but will generally suffer from additional amplifier-induced phase noise. We therefore consider the thermal noise floor for a LO at 0 dBm output as an approximate lower-bound for the phase noise and calculate the resulting upper-bound on operational fidelity in the presence of this noise. Assuming this constant minimal value for the phase noise over frequency, $\tilde{\mathcal{L}}(\omega) = \tilde{\mathcal{L}}_{min}$, the infidelity is computed using $\chi_{min} \approx (\kappa\omega_c/2\pi)10^{\tilde{\mathcal{L}}_{min}/10}$ (see Appendix D). In this expression $\omega_c$ is the cutoff frequency for the control bandwidth, $\kappa$ is a characteristic scaling factor depending on the control protocol, and $\chi_{min}$ is approximately independent of $\tau$ in the limit $\omega_c/2\pi \gg \tau^{-1}$.

This straightforward calculation reveals that broadband noise at room temperature imposes a non-negligible upper bound on gate fidelity as shown in Fig. 3. For a typical 20 GHz bandwidth associated with standard coaxial cable connections between LO and qubit, the thermal noise floor induces qubit infidelity in excess of $10^{-8}$. Reducing the thermal noise floor to that associated with a 4K bath (-192 dBc/Hz) improves the fidelity by two orders of magnitude. Similarly, restricting the control bandwidth to 10 MHz, e.g. via narrowband filtering around the carrier, sets the infidelity $< 10^{-11}$.

| | | Superconducting | Trapped Ion |
|---|---|---|---|
| Lab-Grade | Primitive | $4.1 \times 10^{-8}$ | $7.7 \times 10^{-5}$ |
| | WAMF | $1.5 \times 10^{-11}$ | $2.3 \times 10^{-5}$ |
| Precision | Primitive | $1.9 \times 10^{-10}$ | $8.3 \times 10^{-8}$ |
| | WAMF | $3.4 \times 10^{-13}$ | $4.3 \times 10^{-8}$ |
| 290K (4K) Floor | 100 MHz | $6.3 \times 10^{-11}(1 \times 10^{-12})$ | |
| | 1 GHz | $6.4 \times 10^{-10}\ (1 \times 10^{-11})$ | |
| | 10 GHz | $6.4 \times 10^{-9}\ (1 \times 10^{-10})$ | |

TABLE I. Comparison of typical error rates for superconducting (10 ns) vs trapped-ion (10 $\mu$s) driven-gate operations. Main results calculated assuming an integration bandwidth of 10 MHz. The temperature-dependent noise-floor for different cutoff frequencies is also shown - these data are largely independent of operation time and type. Noise floor calculations strictly valid only for cutoff frequencies high compared with the inverse operation time.

## III. DISCUSSION

The calculations we have presented demonstrate that far-from-carrier phase noise dominates residual errors for commercial sources and is not easily suppressed by DES protocols due to the high-frequency weight in the dephasing power spectrum. Our results enhance existing arguments about the merits of qubit modalities that accommodate fast control pulses; for instance, reducing driven operation times from 10 $\mu$s to 10 ns, upper-bound fidelities can be improved by more than five orders of magnitude for a high-performance synthesizer. Interestingly these example figures represent common operation times for atomic vs solid-state qubits respectively.

However, any move to shorter control operations must be balanced with cognizance of the control *bandwidth*. For example, we indicated that bandwidth-dependent thermal noise floors may pose appreciable upper bounds on operational fidelities. Given the exponential scaling of infidelity with control bandwidth, there is a tradeoff between modulation bandwidth and achievable error rates that must be considered – solely maximizing pulse rates may not ultimately yield optimal performance. In addition, the impact of suppressing the thermal noise floor from -174 dBc/Hz to -192 dBc/Hz suggests that cryogenic LOs [47] embedded in cryogenic control architectures [48] and/or careful cryogenic engineering of amplified room-temperature LOs will play an important role in engineering high-fidelity quantum information systems. We believe it is likely these considerations will have significant bearing on how qubits are connected to classical control electronics and that a detailed cost-benefit analysis will need to be performed weighing operation and modulation rates against added broadband phase noise.

Our observations are particularly concerning because they imply that in many cases clock-induced errors will pose a *lower bound* on error rates feeding into quantum-error correction and fault-tolerance calculations without hardware improvement in a technology space which has received somewhat limited attention. Using precision LOs in most experimental labs will suppress otherwise performance-limiting error rates below currently measurable limits. However, the bounds on error rates associated with both free and driven evolution are, in the view of these authors, remarkably high. Given the efficacy and resource-efficiency of QEC is sensitively dependent to how far the error rate is below the fault-tolerance threshold [49], error floors $\sim 10^{-7}$ for microsecond-scale evolution times using precision LOs make clear the need to focus on developments in advanced master-clock hardware in addition to qubit improvements.

While we have focused on phase fluctuations on short timescales, consideration of both fast phase fluctuations and long-term LO stability is required. It is important to distinguish the impact of long-term instabilities (due to close-to-carrier phase fluctuations) on *experimental measurements* of qubit fidelities from "intrinsic" error rates; the process of data acquisition and averaging over many individual experiments contributes error due to slow drifts that dominate the actual error rate experienced in any *individual* operation (see [22]

for details). In addition, long-time instabilities may be detrimental to systems with multiple control generators, particularly if the generators exhibit phase diffusion with respect to one-another. A detailed accounting of such architectural issues will be the subject of future work.

In summary our results have unified concepts from frequency metrology and quantum information, permitting experimentalists to directly translate common LO hardware specifications into meaningful estimates of qubit coherence and operational fidelities. We have discovered that far-from-carrier phase noise and broadband thermal noise pose a performance limiting upper-bound on operational fidelities, and improving these bounds will require major hardware improvements. As a result we expect to see a growing emphasis on high-performance LO synthesis chains in experimental quantum information laboratories across all technology platforms, and growing importance of LO-induced errors in quantum systems design. Future studies will examine not only clock synthesis, but clock distribution, with an eye towards architectural impacts of clock distribution in quantum systems.

## ACKNOWLEDGMENTS

The authors acknowledge J. J. Bollinger for motivating careful consideration of the role of LO phase noise on qubit coherence and for discussions on phase noise. We acknowledge useful conversations with S. Shankar and R. J. Schoelkopf, who motivated the choice of lab-grade synthesizer. Work partially supported by the ARC Centre of Excellence for Engineered Quantum Systems CE110001013, the Intelligence Advanced Research Projects Activity (IARPA) through the ARO, the US Army Research Office under Contracts W911NF-12-R-0012, and a private grant from H. & A. Harley. The Lincoln Laboratory portion of this work was sponsored by the Assistant Secretary of Defense for Research & Engineering under Air Force Contract #FA8721-05-C-0002. Opinions, interpretations, conclusions and recommendations are those of the author and are not necessarily endorsed by the United States Government.

[1] Ladd T D, Jelezko F, Laflamme R, Nakamura Y, Monroe C and O/'Brien J L 2010 *Nature* **464** 45–53 URL http://dx.doi.org/10.1038/nature08812
[2] Langer C, Ozeri R, Jost J D, Chiaverini J, DeMarco B, Ben-Kish A, Blakestad R B, Britton J, Hume D B, Itano W M, Leibfried D, Reichle R, Rosenband T, Schaetz T, Schmidt P O and Wineland D J 2005 *Phys. Rev. Lett.* **95**(6) 060502 URL http://link.aps.org/doi/10.1103/PhysRevLett.95.060502
[3] Olmschenk S, Younge K C, Moehring D L, Matsukevich D N, Maunz P and Monroe C 2007 *Phys. Rev. A* **76** 052314
[4] Soare A, Ball H, Hayes D, Zhen X, Jarratt M C, Sastrawan J, Uys H and Biercuk M J 2014 *Phys. Rev. A* **89** 042329
[5] Rigetti C, Gambetta J M, Poletto S, Plourde B L T, Chow J M, Córcoles A D, Smolin J A, Merkel S T, Rozen J R, Keefe G A, Rothwell M B, Ketchen M B and Steffen M 2012 *Phys. Rev. B* **86**(10) 100506 URL http://link.aps.org/doi/10.1103/PhysRevB.86.100506
[6] McAuslan D L, Bartholomew J G, Sellars M J and Longdell J J 2012 *Phys. Rev. A* **85**(3) 032339 URL http://link.aps.org/doi/10.1103/PhysRevA.85.032339
[7] Ahlefeldt R, Zhong M, Bartholomew J and Sellars M 2013 *Journal of Luminescence* **143** 193 – 200 ISSN 0022-2313 URL http://www.sciencedirect.com/science/article/pii/S0022231313002573
[8] Muhonen J T, Dehollain J P, Laucht A, Hudson F E, Kalra R, Sekiguchi T, Itoh K M, Jamieson D N, McCallum J C, Dzurak A S and Morello A 2014 *Nature Nanotechnology* **9** 986–991
[9] Brown K R, Wilson A C, Colombe Y, Ospelkaus C, Meier A M, Knill E, Leibfried D and Wineland D J 2011 *Phys. Rev. A* **84**(3) 030303
[10] Kelly J, Barends R, Campbell B, Chen Y, Chen Z, Chiaro B, Dunsworth A, Fowler A, Hoi I C, Jeffrey E, Megrant A, Mutus J, Neill C, O'Malley P, Quintana C, Roushan P, Sank D, Vainsencher A, Wenner J, White T, Cleland A and Martinis J M 2014 *Phys. Rev. Lett.* **112**(24) 240504
[11] Harty T P, Allcock D, Ballance C J, Guidoni L, Janacek H A, Linke N M, Stacey D N and Lucas D M 2014 *Phys. Rev. Lett.* **113**(22) 220501
[12] Fauseweh B, Pasini S and Uhrig G 2012 *Phys. Rev. A* **85** 022310
[13] Green T J, Sastrawan J, Uys H and Biercuk M J 2013 *New J. Phys.* **15** 095004
[14] Biercuk M J, Uys H, VanDevender A P, Shiga N, Itano W M and Bollinger J J 2009 *Nature* **458** 996
[15] Bylander J, Gustavsson S, Yan F, Yoshihara F, Harrabi K, Fitch G, Cory D G, Nakamura Y, Tsai J S and Oliver W D 2011 *Nat. Phys.* **7** 565–570
[16] Soare A, Ball H, Hayes D, Sastrawan J, Jarratt M C, McLoughlin J J, Zhen X, Green T J and Biercuk M J 2014 *Nat. Phys.* **10**
[17] Green T J, Uys H and Biercuk M J 2012 *Phys. Rev. Lett.* **109** 020501
[18] 1990 Characterization of clocks and oscillators Tech. Rep. 1337 National Institute of Standards and Technology
[19] Martinis J M, Nam S, Aumentado J, Lang K M and Urbina C 2003 *Phys. Rev. B* **67** 094510
[20] Uhrig G S 2008 *New J. Phys.* **10** 083024
[21] Biercuk M J, Doherty A C and Uys H 2011 *J. Phys. B* **44** 154002
[22] Yan F, Bylander J, Gustavsson S, Yoshihara F, Harrabi K, Cory D G, Orlando T P, Nakamura Y, Tsai J S and Oliver W D 2012 *Phys. Rev. B* **85**(17) 174521 URL http://link.aps.org/doi/10.1103/PhysRevB.85.174521
[23] Viola L and Lloyd S 1998 *Phys. Rev. A* **58** 2733–2744
[24] Viola L, Lloyd S and Knill E 1999 *Phys. Rev. Lett.* **83** 4888
[25] Zanardi P 1999 *Phys. Lett.* **258** 77
[26] Vitali D and Tombesi P 1999 *Phys. Rev. A* **59** 4178
[27] Viola L and Knill E 2003 *Phys. Rev. Lett.* **90** 037901
[28] Byrd M S and Lidar D A 2003 *Phys. Rev. A* **67** 012324
[29] Kofman A G and Kurizki G 2004 *Phys. Rev. Lett.* **93** 130406
[30] Khodjasteh K and Lidar D A 2005 *Phys. Rev. Lett.* **95** 180501
[31] Yao W, Liu R B and Sham L J 2007 *Phys. Rev. Lett.* **98** 077602
[32] Uhrig G S 2007 *Phys. Rev. Lett.* **98** 100504
[33] Gordon G, Kurizki G and Lidar D A 2008 *Phys. Rev. Lett.* **101** 010403
[34] Khodjasteh K and Viola L 2009 *Phys. Rev. Lett.* **102** 080501

[35] Khodjasteh K and Viola L 2009 *Phys. Rev. A* **80** 032314
[36] Khodjasteh K, Lidar D A and Viola L 2010 *Phys. Rev. Lett.* **104**(9) 090501
[37] Yang W, Wang Z Y and Liu R B 2010 *Frontiers Phys.* **6** 1–13
[38] Biercuk M J, Doherty A C and Uys H 2011 *J. Phys. B* **44** 154002
[39] Ball H and Biercuk M 2015 *EPJ Quantum Technology* **2** 11 URL http://dx.doi.org/10.1140/epjqt/s40507-015-0022-4
[40] Rutman J 1978 *Proceedings of the IEEE* **66** 1048–1075 ISSN 0018-9219
[41] Monroe C and Kim J 2013 *Science* **339** 1164–1169 (*Preprint* http://www.sciencemag.org/content/339/6124/1164.full.pdf) URL http://www.sciencemag.org/content/339/6124/1164.abstract
[42] Oliver W D and Welander P B 2013 *MRS Bulletin* **38**(10) 816–825 ISSN 1938-1425 URL http://journals.cambridge.org/article_S0883769413002297
[43] Reilly D J 2015 *Npj Quantum Information* **1** URL http://dx.doi.org/10.1038/npjqi.2015.11
[44] Khodjasteh K, Sastrawan J, Hayes D, Green T J, Biercuk M J and Viola L 2013 *Nat. Commun.* **4** 2045
[45] Palma M, Suominen K A and Ekert A K 1996 *Proc. R. Soc. London A* **452** 567–584
[46] Hodgson T E, Viola L and D'Amico I 2010 *Phys. Rev. A* **81** 062321
[47] Hartnett J and Nand N 2010 *IEEE Trans. Microwave Thy and Tech.* **58** 3580–3586 ISSN 0018-9480
[48] Hornibrook J, Colless J, Lamb I C, Pauka S, Lu H, Gossard A, Watson J, Gardner G, Fallahi S, Manfra M *et al.* 2015 *Physical Review Applied* **3** 024010
[49] Nielsen M and Chuang I 2010 *Quantum Computation and Quantum Information: 10th Anniversary Edn.* (Cambridge: Cambridge University Press)

## Appendix A: Phase noise in LO upconversion

An experimental LO, operated near resonance with the qubit Larmor frequency will generally be upconverted from a lower-frequency phase reference. This process results in additional phase noise; assuming noiseless upconversion by a factor of $N$ to reach the desired carrier, the carrier phase noise in log units $\mathcal{L}_{\text{carrier}}(\omega) \rightarrow \mathcal{L}_{\text{Ref}}(\omega) + 20 \log N$ dB [18]. The second term on the right indicates that the frequency upconversion leads to an effective increase in the fractional phase instability of the carrier. The synthesis chain will also generally add some phase noise on top of this quantity.

### Appendix B: Analytic forms of filter functions

Here we give the explicit form for the filter-transfer functions for the qubit operations detailed in the main text. Namely, Ramsey (free evolution), spin echo, primitive $\pi$-pulse, and DCG/WAMF $\pi$-pulse. In the dephasing noise quadrature, the filter function in all cases takes the generic form

$$F_z(\omega) = \sum_{l\in\, x,y,z} G_{z,l}(\omega) \tag{B1}$$

where the transfer functions for the control, $G_{z,l}(\omega)$, capture contributions along all Cartesian directions (indexed by $l$). In general all three components are non-zero as dephasing noise induces both dephasing and amplitude-damping rotations [13, 17] during non-commuting control operation (e.g. $H_c \propto \hat{\sigma}_x$).

In the following sections we give the functional form only for the nonzero transfer functions $G_{z,l}(\omega)$ for each of the qubit operations listed above.

#### 1. Ramsey (Spin Echo)

For free evolution (*i.e.* zero driving field) over a duration $\tau$ the only nonzero transfer function component takes the form [15, 19–21]

$$G_{zz}^{(\text{Ramsey})}(\omega) = 4\sin^2\left(\frac{\omega\tau}{2}\right). \tag{B2}$$

#### 2. Spin Echo

Spin echo is the DES version of the identity operation. This takes the form of free evolution over duration $\tau$, but with an instantaneous $\pi_x$ rotation at time $\tau/2$. The nonzero transfer function component takes the form

$$G_{zz}^{(\text{Echo})}(\omega) = \left|1 + e^{i\omega\tau} - 2e^{i\omega\tau/2}\right|^2 = 16\sin^4\left(\frac{\omega\tau}{4}\right). \tag{B3}$$

#### 3. Primitive $\pi$-pulse

For a finite-strength $\pi_x$ rotation of duration $\tau$ and Rabi rate $\Omega = \pi/\tau$, there are two nonzero transfer functions:

$$G_{zz}^{(\pi-\text{Prim})}(\omega) = \left|\frac{\omega^2}{\omega^2-\Omega^2}\left(e^{i\omega\tau}+1\right)\right|^2, \tag{B4}$$

$$G_{zy}^{(\pi-\text{Prim})}(\omega) = \left|\frac{i\omega\Omega}{\omega^2-\Omega^2}\left(e^{i\omega\tau}+1\right)\right|^2. \tag{B5}$$

The second line arises because of the noncommuting nature of the control ($\propto \hat{\sigma}_x$) and the dephasing noise ($\propto \hat{\sigma}_z$), as described in [13, 17].

#### 4. DCG/WAMF $\pi$-pulse

This is a finite-strength sequence performing a net $\pi$ rotation and defined both as a *dynamically corrected gate* (DCG) and a *Walsh amplitude modulated filter* (WAMF) [16, 39]. Let $\hat{R}_x(\theta,\tau)$ be a non-instantaneous qubit rotation about $\hat{\sigma}_x$ on the Bloch sphere, through an angle $\theta$ over a duration $\tau$ (*i.e.* with Rabi rate $\Omega = \theta/\tau$). Then the DCG/WAMF sequence of total duration $\tau$ is defined by the operator sequence

$$\hat{R}_x\left(\pi,\frac{\tau}{4}\right)\hat{R}_x\left(\pi,\frac{\tau}{2}\right)\hat{R}_x\left(\pi,\frac{\tau}{4}\right), \tag{B6}$$

with transfer function components

$$G_{zy}(\omega) = \left|\frac{i4\pi\omega\tau e^{i\frac{\omega\tau}{2}}\left[\left(\tau^2\omega^2+8\pi^2\right)\cos\left(\frac{\omega\tau}{4}\right)+2\left(\tau^2\omega^2-4\pi^2\right)\cos\left(\frac{\omega\tau}{2}\right)\right]}{\tau^4\omega^4-20\pi^2\tau^2\omega^2+64\pi^4}\right|^2, \tag{B7}$$

$$G_{zz}(\omega) = \left|\frac{2\tau^2\omega^2 e^{i\frac{\omega\tau}{2}}\left[12\pi^2\cos\left(\frac{\omega\tau}{4}\right)+\left(\tau^2\omega^2-4\pi^2\right)\cos\left(\frac{\omega\tau}{2}\right)\right]}{\tau^4\omega^4-20\pi^2\tau^2\omega^2+64\pi^4}\right|^2. \tag{B8}$$

### Appendix C: Relationship between $S_z(\omega)$ and $S_{\phi_N}(\omega)$

#### 1. Definition of PSD (Bilateral)

Let $y(t)$ denote a real-valued stochastic process defined continuously on the time domain. For a set $\mathcal{E}$ of individual realizations of this process, let $y_k(t)$, $k \in \mathcal{E}$, denote the $k$th realization. Further, let $Y_{k,t} \equiv y_k(t)$ denote the (scalar) random variable taking the value of the $k$th realization at fixed time $t$. We introduce the following notation to distinguish between the *ensemble* average and the *time* average:

$$\langle y(t)\rangle \equiv \lim_{|\mathcal{E}|\to\infty}\frac{1}{|\mathcal{E}|}\sum_{k\in\mathcal{E}} Y_{k,t} \qquad (\textit{ensemble average}), \tag{C1}$$

$$\overline{y_k(t)} \equiv \lim_{T\to\infty}\frac{1}{T}\int_0^T y_k(t)dt \quad (\textit{time average}), \tag{C2}$$

where $|\mathcal{E}|$ is the number of elements in the set $\mathcal{E}$. We include explicitly the subscript $k$ in the expression for the time average to emphasize that it is computed over a *single* realization of $y(t)$. We assume the following properties of $y(t)$:

1. $y(t)$ is a wide-sense stationary (w.s.s.) process.

2. $y(t)$ is an ergodic process.

3. $y(t)$ is a zero-mean process: $\langle y(t)\rangle = \overline{y_k(t)} = 0, \forall t$.

By w.s.s. we mean the ensemble autocorrelation function $C_y(\tau)$ is invariant under time-translations of $\tau$. By ergodic we mean that, in the limit of infinite ensemble sizes, the ensemble mean of $y(t)$ – or the ensemble mean of a function of $y(t)$ – approaches the corresponding *time-average* over any given realization $y_k(t)$. That is,

$$\langle f(y(t))\rangle \longleftrightarrow \overline{f(y_k(t))}. \tag{C3}$$

In particular, ergodicity permits the autocorrelation function to be equivalently defined either in terms of the ensemble average or the time average

$$C_y(\tau) = \langle y(t)y(t+\tau)\rangle = \overline{y_k(t)y_k(t+\tau)}. \tag{C4}$$

Due to the assumption of w.s.s. the autocorrelation function above depends only on the time *difference*, $\tau$, between measurements. We now define the truncated Fourier transform of $y(t)$ by

$$Y_T(\omega) \equiv \int_{-T}^{T} y(t)e^{-i\omega t}dt, \tag{C5}$$

where the *angular frequency, non-unitary* convention for Fourier transforms has been used. This definition avoids the difficulty that the full Fourier transform may not be well defined if the integral over $y(t)$ fails to converge in the limit $T \to \infty$. The power spectral density (PSD) of $y(t)$ may then be defined by

$$S_y(\omega) = \lim_{T\to\infty} \frac{1}{2T}\left\langle |Y_T(\omega)|^2 \right\rangle. \tag{C6}$$

Writing this out we explicitly we obtain

$$S_y(\omega) = \lim_{T\to\infty} \frac{1}{2T}\left\langle \int_{-T}^{T} y^*(t)e^{i\omega t}dt \int_{-T}^{T} y(t')e^{-i\omega t'}dt' \right\rangle \tag{C7}$$

$$= \lim_{T\to\infty} \frac{1}{2T}\int_{-T}^{T}\int_{-T}^{T} \langle y(t)y(t')\rangle\, e^{i\omega(t-t')}dtdt' \tag{C8}$$

$$= \lim_{T\to\infty} \frac{1}{2T}\int_{-T}^{T}\int_{-T}^{T} C_y(\tau)e^{-i\omega\tau}dtdt', \tag{C9}$$

where we have used the fact that $y(t)$ is real, and defined the new variable $\tau = t' - t$. Transforming the integral domain we get

$$S_y(\omega) = \lim_{T\to\infty} \frac{1}{2T}\int_{-2T}^{2T} (2T - |\tau|)C_y(\tau)e^{-i\omega\tau}d\tau \tag{C10}$$

$$= \lim_{T\to\infty} \int_{-2T}^{2T} C_y(\tau)e^{-i\omega\tau}d\tau \tag{C11}$$

$$+ \lim_{T\to\infty} \frac{1}{2T}\int_{-2T}^{2T} |\tau|\, C_y(\tau)e^{-i\omega\tau}d\tau. \tag{C12}$$

Assuming $y(t)$ has *finite* temporal correlations, appropriate for realistic physical processes, the autocorrelation function $C_y(\tau)$ vanishes in the limit $\tau \to \infty$. Consequently the second term above vanishes in the limit $T \to \infty$ yielding

$$S_y(\omega) = \int_{-\infty}^{\infty} C_y(\tau)e^{-i\omega\tau}d\tau, \tag{C13}$$

$$C_y(\tau) = \frac{1}{2\pi}\int_{-\infty}^{\infty} S_y(\omega)e^{i\omega\tau}d\omega. \tag{C14}$$

That is, $S_y(\omega)$ and $C_y(\tau)$ form a Fourier transform pair, which is a statement of the Wiener-Khintchine theorem.

### 2. Bilateral and Unilateral PSDs

The power spectral density formulated in Eq. C6 is by definition a non-negative even function on the real domain $\omega \in (-\infty, \infty)$. This is known as the *bilateral* PSD, with total power (or mean-square fluctuation) given by integrating over both positive and negative frequency domain:

$$P_{\text{tot}} = C_y(0) = \left\langle y(t)^2 \right\rangle \tag{C15}$$

$$= \frac{1}{2\pi}\int_{-\infty}^{\infty} S_y(\omega)d\omega \tag{C16}$$

$$= \int_{-\infty}^{\infty} S_y(\nu)d\nu, \quad \omega = 2\pi\nu. \tag{C17}$$

The bilateral PSD naturally arises in mathematical analysis involving Fourier transformations, satisfying the Wiener-Khinchine theorem describing its relationship with the autocorrelation function $C_y(\tau)$ in Eqs. C13 and C14.

It is also useful when considering systems subject to quantum noise, for which the corresponding quantum operator $\hat{y}(t)$ in general does not commute at different times and is in principle a complex number, i.e., $\langle \hat{y}(t)\hat{y}(t+\tau)\rangle = a + ib$. The spectral density of a complex number is no longer an even function in $\omega$ so must be specified for both positive and negative frequencies. Such non-symmetric spectra arise, for example, in the context of qubit stimulated and spontaneous emission and absorption to/from the environment.

For real-valued $y(t)$, however, the bilateral PSD is symmetric and may be replaced by the *unilateral* PSD, more typically used in engineering and metrological applications dealing with manifestly classical signals. Environmental fluctuations responsible for qubit dephasing fall into this category. For clarity, in this paper we use the following notation to keep

the usage of bilateral (two-sided) and unilateral (one-sided) PSDs distinct:

$$S_y^{(2)}(\omega) \qquad (\textit{bilateral}), \tag{C18}$$

$$S_y^{(1)}(\omega) \qquad (\textit{unilateral}), \tag{C19}$$

where the unilateral PSD is defined by

$$S_y^{(1)}(\omega) = \begin{cases} 2S_y^{(2)}(\omega) & \text{for } \omega \geq 0 \\ 0 & \text{for } \omega < 0 \end{cases}. \tag{C20}$$

With these definitions the total power in the signal is given by

$$P_{\text{tot}} = \int_{-\infty}^{\infty} S_y^{(2)}(\nu) d\nu \tag{C21}$$

$$= 2\int_{0}^{\infty} S_y^{(2)}(\nu) d\nu \tag{C22}$$

$$= \int_{0}^{\infty} S_y^{(1)}(\nu) d\nu. \tag{C23}$$

### 3. PSDs for Phase and Frequency Noise

Consider a local oscillator

$$\Omega(t)\cos[\omega_{\text{LO}} t + \phi_N(t)] \tag{C24}$$

with instantaneous frequency

$$\omega(t) \equiv \frac{d}{dt}\left[\omega_{\text{LO}} t + \phi_N(t)\right] = \omega_{\text{LO}} + \dot{\phi}_N(t), \tag{C25}$$

or

$$\omega(t) = \omega_{\text{LO}} + \delta\omega_{\text{LO}}(t) \tag{C26}$$

where the (angular) frequency noise takes the form

$$\delta\omega_{\text{LO}}(t) = \dot{\phi}_N(t). \tag{C27}$$

Following Eq. C5 we define the truncated Fourier transforms for phase and frequency noise fields

$$\Phi_T(\omega) \equiv \int_{-T}^{T} \phi_N(t) e^{-i\omega t} dt, \tag{C28}$$

$$W_T(\omega) \equiv \int_{-T}^{T} \delta\omega_{\text{LO}}(t) e^{-i\omega t} dt. \tag{C29}$$

Then the phase and frequency noise PSDs are defined by

$$S_{\phi_N}(\omega) = \lim_{T\to\infty} \frac{1}{2T}\left\langle |\Phi_T(\omega)|^2 \right\rangle, \tag{C30}$$

$$S_{\delta\omega_{\text{LO}}}(\omega) = \lim_{T\to\infty} \frac{1}{2T}\left\langle |W_T(\omega)|^2 \right\rangle. \tag{C31}$$

Using the definition of $\Phi_T(\omega)$, the fact that $\delta\omega_{\text{LO}}(t) = \dot{\phi}_N(t)$, and integrating by parts we find

$$W_T(\omega) = i\omega\Phi_T(\omega) + R, \tag{C32}$$

$$R \equiv \phi_N(T)e^{-i\omega T} - \phi_N(-T)e^{i\omega T}, \tag{C33}$$

where the residual term $R$ comes from the integration limits after integrating by parts, and we have used the Fourier relation $d/dt \leftrightarrow i\omega$. Taking the modulus square we therefore obtain

$$|W_T(\omega)|^2 = \omega^2 |\Phi_T(\omega)|^2 + R', \tag{C34}$$

where the residual terms are absorbed into

$$R' = |R|^2 + [i\omega\Phi_T(\omega)R^*] + [-i\omega\Phi_T(\omega)^* R]. \tag{C35}$$

Consequently

$$S_{\delta\omega_{\text{LO}}}(\omega) = \lim_{T\to\infty} \frac{1}{2T}\left\langle \omega^2 |\Phi_T(\omega)|^2 + R' \right\rangle \tag{C36}$$

$$= \omega^2 \left[\lim_{T\to\infty} \frac{1}{2T}\left\langle |\Phi_T(\omega)|^2 \right\rangle\right] + \lim_{T\to\infty} \frac{1}{2T}\langle R' \rangle. \tag{C37}$$

The term in square brackets is the definition of $S_{\phi_N}(\omega)$. The second term, on the other hand, vanishes in the limit $T \to \infty$ as the residual term $R'$ does not grow sufficiently rapidly with $T$. We therefore set

$$\lim_{T\to\infty} \frac{1}{2T}\langle R' \rangle = 0 \tag{C38}$$

from which it follows

$$S_{\delta\omega_{\text{LO}}}(\omega) = \omega^2 S_{\phi_N}(\omega). \tag{C39}$$

Now define the noise field

$$\beta(t) \equiv \alpha\delta\omega_{\text{LO}}(t) = \alpha\dot{\phi_N}(t) \tag{C40}$$

by simply scaling the frequency noise by some factor $\alpha$. Substituting this into the above derivation we obtain the slightly more general PSD relation

$$S_\beta(\omega) = \alpha^2 S_{\delta\omega_{\text{LO}}} = \alpha^2\omega^2 S_{\phi_N}(\omega). \tag{C41}$$

These relations apply to bilateral and unilateral PSDs.

### 4. Interpretation of $S_{\phi_N}(\omega)$: Sideband and Modulation Theory

Here we provide an interpretation of the phase instability $S_{\phi_N}(\omega)$ defined in Eq. 10 as the ratio of the power in the sidebands relative to the power in the carrier. Consider the LO signal

$$V(t) = \Omega\cos[\omega_{\text{LO}} t + \phi_N(t)], \tag{C42}$$

where in a given realization, over some window $[-T, T]$, $\phi_N(t)$ has spectral components described by some Fourier spectrum. To obtain a simple interpretation of the resulting PSD $S_{\phi_N}(\omega)$, we restrict attention to the case where $\phi_N(t)$ consists of a single (phase-randomized) Fourier component

$$\phi_N(t) = \frac{\alpha_j}{2}\left(e^{i\omega_j t+\psi_j} + \text{c.c.}\right) = \alpha_j \cos(\omega_j t + \psi_j), \quad \text{(C43)}$$

equivalent to imposing a narrow-band filter at Fourier frequency $\omega_j$. The resulting waveform may be expressed in terms of an infinite comb of frequency components,

$$V(t) = \Omega \sum_{n=-\infty}^{\infty} J_n(\alpha_j)\cos[(\omega_{\text{LO}} + n\omega_j)t + n\psi_j], \quad \text{(C44)}$$

weighted by Bessel functions $J_n(x)$ and centred around the carrier frequency $\omega_{\text{LO}}$. Assuming the phase fluctuations are small relative to the carrier frequency ($\alpha_j \ll \omega_{\text{LO}}$) we may make the *small angle approximation* to obtain

$$V(t) \approx V_0(t) + V_+(t) + V_-(t), \quad \text{(C45)}$$

where

$$V_0(t) \equiv \Omega\cos(\omega_{\text{LO}}t) \quad \textit{(LO/carrier)}, \quad \text{(C46)}$$

$$V_+(t) \equiv \frac{\Omega}{2}\alpha_j\cos[(\omega_+ t + \psi_j)] \quad \textit{(right sideband)}, \quad \text{(C47)}$$

$$V_-(t) \equiv \frac{\Omega}{2}\alpha_j\cos[(\omega_- t - \psi_j)] \quad \textit{(left sideband)}, \quad \text{(C48)}$$

and $\omega_\pm \equiv \omega_{\text{LO}} \pm \omega_j$ are the positive- and negative-detuned frequencies of the principle (first-order) sidebands on the carrier. Using Eqs. C5 and C6 we may now compute the PSDs for $\phi_N(t)$, $V_0(t)$ and $V_\pm(t)$.

Substituting Eq. C43 into Eq. C5, the truncated Fourier transform of the phase fluctuation is given by

$$\Phi_T(\omega) = \alpha_j T\left(e^{i\psi_j}\text{sinc}[T(\omega-\omega_j)] + e^{-i\psi_j}\text{sinc}[T(\omega+\omega_j)]\right).$$

Using Eq. C6 the (bilateral) PSD is therefore given by

$$\begin{aligned} S^{(2)}_{\phi_N}(\omega) &= \lim_{T\to\infty}\frac{1}{2T}\left\langle|\Phi_T(\omega)|^2\right\rangle \\ &= \lim_{T\to\infty}\frac{T\alpha_j^2}{2}\left(\text{sinc}^2[T(\omega-\omega_j)] + \text{sinc}^2[T(\omega+\omega_j)]\right), \end{aligned}$$

where cross products in the modulus square between the *different* frequency components, $\text{sinc}[T(\omega \pm \omega_j)]$, are omitted as these vanish in the limit $T \to \infty$. Carrying out the limit, subject to the condition that the area under the $\text{sinc}^2(x)$ curve remains equal to $\pi$, we obtain

$$S^{(2)}_{\phi_N}(\omega) = \frac{\pi}{2}\alpha_j^2\left[\delta(\omega-\omega_j) + \delta(\omega+\omega_j)\right]. \quad \text{(C49)}$$

Similarly,

$$S^{(2)}_{V_0}(\omega) = \frac{\pi}{2}\Omega^2\left[\delta(\omega-\omega_{\text{LO}}) + \delta(\omega+\omega_{\text{LO}})\right], \quad \text{(C50)}$$

$$S^{(2)}_{V_\pm}(\omega) = \frac{\pi}{2}\left(\frac{\Omega\alpha_j}{2}\right)^2\left[\delta(\omega-\omega_\pm) + \delta(\omega+\omega_\pm)\right]. \quad \text{(C51)}$$

Let $P_y(\omega, \Delta)$ denote the power in the signal $y(t)$ in (angular) frequency bandwidth $\Delta$ centred on (angular) frequency $\omega$, namely over bandwidth $[\omega - \Delta/2, \omega + \Delta/2]$. Then

$$P_y(\omega,\Delta) = \frac{1}{2\pi}\int_{\omega-\Delta/2}^{\omega+\Delta/2} 2S^{(2)}_y(\omega')d\omega', \quad \text{(C52)}$$

where the factor of 2 inside the integral accounts for the equal contribution to the total power in this bandwidth from the negative frequency domain of the bilateral PSD. In our case, for any $\Delta > 0$, we obtain

$$P_{\phi_N}(\omega_j,\Delta) = \frac{1}{2}\alpha_j^2, \quad \text{(C53)}$$

$$P_{V_0}(\omega_{\text{LO}},\Delta) = \frac{1}{2}\Omega^2, \quad \text{(C54)}$$

$$P_{V_\pm}(\omega_\pm,\Delta) = \frac{1}{2}\left(\frac{\Omega\alpha_j}{2}\right)^2. \quad \text{(C55)}$$

The ratio of the total power *in both sidebands* relative to the carrier is therefore given by

$$\frac{P_{V_+}(\omega_+,\Delta) + P_{V_-}(\omega_-,\Delta)}{P_{V_0}(\omega_{\text{LO}},\Delta)} = \frac{1}{2}\alpha_j^2 = P_{\phi_N}(\omega_j,\Delta). \quad \text{(C56)}$$

In particular, setting $\Delta = 1/2\pi$ rad $= 1$ Hz and dividing the power by the measurement bandwidth, we obtain

$$\frac{P_{\phi_N}(\omega_j,\Delta)}{\Delta} = \pi\alpha_j^2 \quad [\text{rad}^2/\text{rad}]. \quad \text{(C57)}$$

Using Eq. C49, this compares directly with the (unilateral) PSD for $\phi_N(t)$ (i.e. the phase instability)

$$S^{(1)}_{\phi_N}(\omega) = \pi\alpha_j^2\delta(\omega-\omega_j). \quad \text{(C58)}$$

Consequently, $S^{(1)}_{\phi_N}(\omega)$ may be interpreted, according to Eq. C56, as the ratio of the power in the sidebands relative to the power in the carrier measured over a 1 Hz bandwidth.

## Appendix D: Thermal noise floor

Here we consider the contribution to infidelity from the fundamental limit associated with a thermal noise floor. The theoretical minimum noise power for an oscillator coupled into 50 Ω cable is $kTB$ for bandwidth $B$, temperature $T$, and where $k$ is the Boltzmann constant. Normalized to a 1Hz bandwidth this is expressed in dBm/Hz (Table II).

| $T\,[K]$ | $\tilde{\mathcal{L}}_{min}$ [W/Hz] | $\tilde{\mathcal{L}}_{min}$ [dBm/Hz] |
|---|---|---|
| 4 | $4\times10^{-21}$ | $-174$ |
| 290 | $4\times10^{-21}$ | $-192$ |

TABLE II. Lower bounds on phase noise set by thermal noise floor.

We assume an oscillator at 0 dBm where the minimal phase noise is given by the power in the thermal noise referenced to the power in the carrier. We impose a high-frequency cutoff $\omega_c$ on to the otherwise white thermal noise to account for filtering due to e.g. coaxial cable cutoff frequencies or narrowband filtering. Hence, the thermal noise floor may be characterized by

$$\tilde{\mathcal{L}}(\omega) = \begin{cases} \tilde{\mathcal{L}}_{min} & 0 \le \omega \le \omega_c \\ 0 & \omega > \omega_c \end{cases}. \tag{D1}$$

The infidelity $\mathcal{I} = 1 - \mathcal{F}$ associated with this noise floor is given by

$$\mathcal{I} = 1 - \frac{1}{2}\Big[1 + e^{-\chi(\tau)}\Big], \tag{D2}$$

where

$$\chi(\tau) = \frac{1}{2\pi}\int_0^\infty d\omega 10^{\frac{\tilde{\mathcal{L}}(\omega)}{10}} F_z(\omega) \tag{D3}$$

$$= \frac{1}{2\pi}10^{\frac{\tilde{\mathcal{L}}_{min}}{10}}\int_0^{\omega_c} d\omega F_z(\omega) \tag{D4}$$

and $F_z(\omega) = \sum_{l\in\, x,y,z} G_{z,l}(\omega)$ is the filter function. Thus, the infidelity is given by the integral of the filter function over the band $[0,\omega_c]$ scaled by a constant factor associated with the strength of the thermal noise floor. For the qubit operations described in the main text we can obtain analytic expressions for this integral. We assume the cutoff frequency $\omega_c$ is fast compared to the duration $\tau$ of the qubit operation:

$$\omega_c \gg \frac{1}{\tau} \iff \omega_c\tau \gg 1. \tag{D5}$$

In this case the bulk of the thermal noise floor lies in the bandwidth beyond the stopband of the filter function and the integral is very well approximated by its asymptotic value, linear in the cutoff frequency. Specifically

$$\chi(\tau) = \frac{\kappa\omega_c}{2\pi}10^{\frac{\tilde{\mathcal{L}}_{min}}{10}}, \tag{D6}$$

where

$$\kappa = 2 \qquad (\textit{Ramsey}), \tag{D7}$$

$$\kappa = 6 \qquad (\textit{spin echo}), \tag{D8}$$

$$\kappa = 2 \qquad (\textit{primitive } \pi\textit{-pulse}), \tag{D9}$$

$$\kappa = 2 \qquad (\textit{DCG/WAMF } \pi\textit{-pulse}). \tag{D10}$$

We derive these expressions below.

### 1. Ramsey (Free Evolution)

In the case of free evolution we have

$$\int_0^{\omega_c} d\omega F_z(\omega) = \int_0^{\omega_c} 4\sin\left(\frac{\omega\tau}{2}\right)^2 d\omega \tag{D11}$$

$$= 2\omega_c\left(1 - \frac{\sin(\omega_c\tau)}{\omega_c\tau}\right) \tag{D12}$$

$$\approx 2\omega_c, \qquad \omega_c\tau \gg 1. \tag{D13}$$

Consequently

$$\chi(\tau) = \frac{1}{2\pi}10^{\frac{\tilde{\mathcal{L}}_{min}}{10}}(2\omega_c) \qquad (\textit{Ramsey}) \tag{D14}$$

is proportional to the cutoff, with proportionality factor associated with strength of the thermal noise floor. Using the appropriate filter function, similar results hold for other qubit operations.

### 2. Spin Echo

For the spin echo sequence it is just as straightforward to derive

$$\int_0^{\omega_c} d\omega F_z(\omega) = 6\omega_c. \tag{D15}$$

Hence

$$\chi(\tau) = \frac{1}{2\pi}10^{\frac{\tilde{\mathcal{L}}_{min}}{10}}(6\omega_c) \qquad (\textit{spin echo}). \tag{D16}$$

### 3. Primitive $\pi$-pulse

The form of the filter function gets rapidly more complicated for finite-width pulses. For the primitive $\pi$ pulse we have

$$F_z(\omega) = \frac{2\pi^2 z^2}{(\pi^2 - z^2)^2} + \frac{2z^4}{(\pi^2 - z^2)^2} + \frac{2\pi^2 z^2\cos(z)}{(\pi^2 - z^2)^2} + \frac{2z^4\cos(z)}{(\pi^2 - z^2)^2}, \tag{D17}$$

where we introduce the dimensionless variable $z = \omega\tau$. The main contribution to the integral over the band $[0,\omega_c]$ for $\omega_c \gg 1/\tau$ comes from those terms in Eq. D17 which sur-

vive the limit $z \to \infty$. We find

$$\lim_{z\to\infty} \frac{2\pi^2 z^2}{(\pi^2 - z^2)^2} = 0,$$
$$\lim_{z\to\infty} \frac{2z^4}{(\pi^2 - z^2)^2} = 2,$$
$$\lim_{z\to\infty} \frac{2\pi^2 z^2 \cos(z)}{(\pi^2 - z^2)^2} \to \left[\lim_{z\to\infty} \frac{2\pi^2 z^2}{(\pi^2 - z^2)^2}\right] \cos(z) = 0,$$
$$\lim_{z\to\infty} \frac{2z^4 \cos(z)}{(\pi^2 - z^2)^2} \to \left[\lim_{z\to\infty} \frac{2z^4}{(\pi^2 - z^2)^2}\right] \cos(z) = 2\cos(z),$$

where in the last two lines we formally separate the oscillating (and bounded) cosine factors in order to extract the *functional* form of the surviving terms. Consequently,

$$F_z(\omega) \approx 2\left(1 + \cos(\omega\tau)\right), \qquad \omega\tau \gg 1, \tag{D18}$$

and the integral is well approximated by

$$\int_0^{\omega_c} F_z(\omega)d\omega \approx \int_0^{\omega_c} 2\left(1 + \cos(\omega\tau)\right) d\omega \tag{D19}$$
$$= \omega_c \left(2 + \frac{\sin(\omega_c\tau)}{\omega_c\tau}\right) \tag{D20}$$
$$\approx 2\omega_c, \qquad \omega_c\tau \gg 1. \tag{D21}$$

Hence

$$\chi(\tau) = \frac{1}{2\pi} 10^{\frac{\bar{c}_{min}}{10}} (2\omega_c) \qquad (\textit{primitive } \pi\textit{-pulse}). \tag{D22}$$

#### 4. DCG/WAMF $\pi$-pulse

Similarly, expanding the filter function for DCG/WAMF $\pi$-pulse and taking the limit, the only surviving term takes the form

$$\lim_{z\to\infty} \frac{4z^8 \cos(\frac{z}{2})^2}{(64\pi^4 - 20\pi^2 z^2 + z^4)^2} \to 4\cos^2\left(\frac{z}{2}\right). \tag{D23}$$

Consequently,

$$F_z(\omega) \approx 4\cos^2\left(\frac{\omega\tau}{2}\right), \qquad \omega\tau \gg 1, \tag{D24}$$

and the integral is well approximated by

$$\int_0^{\omega_c} F_z(\omega)d\omega \approx \int_0^{\omega_c} 4\cos^2\left(\frac{\omega\tau}{2}\right) d\omega \tag{D25}$$
$$= 2\omega_c \left(1 + \frac{\sin(\omega_c\tau)}{\omega_c\tau}\right) \tag{D26}$$
$$\approx 2\omega_c, \qquad \omega_c\tau \gg 1. \tag{D27}$$

Hence

$$\chi(\tau) = \frac{1}{2\pi} 10^{\frac{\bar{c}_{min}}{10}} (2\omega_c) \qquad (\textit{DCG/WAMF } \pi\textit{-pulse}). \tag{D28}$$